Capacitive Removal of Heavy Metal Ions from Wastewater *via* an Electro-Adsorption and Electro-Reaction Coupling Process

Minlin Mao[†], Tingting Yan[†], Junjie Shen[‡], Jianping Zhang[†], and Dengsong Zhang[†*]

[†]*State Key Laboratory of Advanced Special Steel, School of Materials Science and Engineering, International Joint Laboratory of Catalytic Chemistry, Research Center of Nano Science and Technology, Department of Chemistry, College of Sciences, Shanghai University, No.99 Shangda Road, Shanghai, 200444, China.*

[‡]*Department of Chemical Engineering, University of Bath, Bath BA2 7AY, UK.*

[*] *E-mail: dszhang@shu.edu.cn; Tel: +86 21 66137152.*

ABSTRACT:

Heavy metals widely exist in in wastewater, which is a serious threat to human health or water environment. Highly efficient removal of heavy metal ions from wastewater is a major challenge to wastewater treatment. In this work, capacitive removal of heavy metal ions from wastewater via an electro-adsorption and electro-reaction coupling process was originally demonstrated. The removal efficiency of heavy metal ions in the binary-component solutions containing metal nitrate (10 mg/L) and NaCl (100 mg/L) can reach 99%. Even the removal efficiency of heavy metal ions can be close to 99% in the multi-component solution containing all the seven metal nitrates (10 mg/L for each) and 100 mg/L NaCl. Meanwhile, the electro-adsorption and electro-reaction coupling process maintained excellent regeneration ability even after 20 cycles. Furthermore, the heavy metal ions removal mechanism was proven to be the pseudocapacitive intercalation of heavy metal ions into the layered structure of the employed $W_{18}O_{49}$/Graphene in the electro-adsorption and electro-reaction coupling

process. This work demonstrates great potential for general applicability to wastewater treatment.

Introduction

Globally, water scarcity has become a key challenge for sustainable development. This challenge will become more pressing due to increasing water demand and ubiquitous water pollution, driven by rapid population growth and economic development.[1, 2] Heavy metals are highly toxic and exist in wastewater, which is a serious threat to human health or water environment. Recently, a variety of effective methods have been developed to remove heavy metal ions from water, such as adsorption, chemical precipitation, ion exchange and membrane separation.[3-6] However, these methods require the addition of environmentally unfriendly chemicals and excessive pretreatment steps. Hence, it is very necessary to design an efficient means for removal of heavy metals for the sustainable development of the environment.

Electro-adsorption is an emerging electrochemical desalination technology which has the advantages of high energy efficiency, low environmental impact and low cost.[7-9] In a typical electro-adsorption process, two porous electrodes are arranged in parallel and an aqueous solution flow between them. An electric field is established when a certain voltage is applied between the two electrodes. The charged ions in the solution move to the surface of the oppositely charged electrodes via the electric field force, and are finally adsorbed in the pores of the electrodes, thus reducing the overall concentration of ions in the solution.[10-12] When the voltage is removed or reversed, the adsorbed ions are released into the solution and the electrodes are thus regenerated. [13-21] The removal ion ability of an electro-adsorption system largely depends on the electrical double layer (EDL) at the interface.[22-35] Graphene is a two-dimensional carbon material with good conductivity, high hydrophilicity, and

large theoretical capacitance.[36, 37] Various modified graphene composites have been developed at the electro-adsorption systems.[38-40] However, these graphene composites suffer from low removal ability and excessive co-ion discharge due to the intrinsic limitation of electro-sorption, which hinders their practical applications in wastewater treatment. The introduction of electro-reaction significantly improves the removal ion ability. Unlike porous carbon electrodes which store ions in the EDL, electro-reaction store ions via electrochemical process. Su et al.[41] reported a kind of redox-active polymer electrodes for capacitive removal of heavy metal ions. The results show that it has a high adsorption and conversion capacity for As(III) in wastewater. We reported the capacitive removal of Pb in wastewater via MoO_2/C electrodes[42]. The electrodes have high removal efficiency in the mixtures of NaCl and Pb $(NO_3)_2$. The electro-reaction process mainly includes ion intercalation and conversion.[43-49] The conversion reaction means that the material can react with anions to form a new phase, and the conversion material can remove anions by using a suitable dual-channel deionization system. The intercalation reaction is to insert cations or anions into specific or non-specific interstitial positions of the electrode material, so as to realize the storage of ions. However, the adsorption and desorption of ions through the conversion electro-reaction process can easily lead to volume change, resulting in serious attenuation and poor stability. [45] Using intercalation electro-reaction process can avoid the above shortcomings. [43, 50-52] This is because the larger interlayer spacing of intercalation electrodes can provide larger ion storage spaces, thus effectively improving the reversible capacity of electro-reaction. Therefore, how to design highly efficient capacitive removal of heavy metal ions from wastewater is still a challenge.

$W_{18}O_{49}$ has a high specific capacitance and an adjustable interlayer spacing, which can facilitate ion transport[53, 54] and improve the reversibility of electrosorption.[55] The synthesis process of $W_{18}O_{49}$

material is simple and has no stacking problem, and it doesn't even react with acidic or alkaline solutions. Besides, the mixed valence state of W^{4+}, W^{5+} and W^{6+} in the $W_{18}O_{49}$ lattice results in local residual electrons and lattice distortion, which accumulates a large number of free electrons on the surface, resulting in an electron affinity for heavy metal ions. However, the single-component $W_{18}O_{49}$ is limited by the low electrical conductivity and low specific surface area. The combination of $W_{18}O_{49}$ and graphene can provide a highly conductive matrix for the electrode. More importantly, the $W_{18}O_{49}$/Graphene composite can obtain a significantly improved the ability of ion removal through the electro-adsorption and electro-reaction coupling process.

Herein, highly efficient capacitive removal of heavy metal ions from wastewater via an electro-adsorption and electro-reaction coupling process by using $W_{18}O_{49}$/Graphene intercalation materials was originally demonstrated. The $W_{18}O_{49}$/Graphene electrode exhibited remarkably high removal efficiency of various heavy metal ions in the single, binary, and multi-component synthetic wastewater via the pseudocapacitive intercalation electro-reaction process and has excellent recyclability after 20 cycles. Using in-situ Raman spectroscopy and other analytical techniques, we observe the insertion and extraction reaction of heavy metal ions over $W_{18}O_{49}$/Graphene. The electro-adsorption and electro-reaction coupling process demonstrates great potential for general applicability to wastewater treatment.

Experimental section

Preparation. $(NH_4)_{10}W_{12}O_{41}{\sim}xH_2O$ (1.2 g) and graphene (0.1 g) were poured into 100 mL (pH = 8.5) tris-buffer solutions (The tris-buffer solutions preparation is described in Supporting Information) with a 5-min ultrasonic treatment. The mixtures were heated to 80°C while stirring for 30 min. 0.4 g of dopamine hydrochloride was dissolved in the above mixtures and stirred for 120 min. 160 mL of

CH_3CH_2OH was poured into the suspension via stirring 60 min. Moreover, $NH_3 \cdot H_2O$ (1.2 mL) was added to the above solutions via stirring 120 min, then centrifuged with ethanol, washed, and dried 12 h. The mixtures were carbonized in a nitrogen atmosphere at 750°C for 3 h (5 °C min^{-1}) to obtain $W_{18}O_{49}$/Graphene. In capacitive deionization system ($W_{18}O_{49}$/Graphene||AC), the activated carbon (AC) was used to the anode and $W_{18}O_{49}$/Graphene was used to the cathode. More experiment details or characterization can be found in the Supporting Information.

Electrochemical Experiments. The prepared material (5 mg), polytetrafluoroethylene (PTFE) and conductive carbon black were fully mixed at an 8:1:1 mass ratio to make the film, which was cast on graphite film (GF) collector to make the experimental working electrode. The galvanostatic charge−discharge (GCD) curves and Cyclic voltammetry (CV) and electrochemical impedance spectroscopy (EIS) were measured via the three-electrode system in the 1000 mg/L NaCl solutions. Calomel electrode is reference electrode and GF is counter electrode. More experiment details are provided in Supporting Information.

Capacitive Removal Experiments. A capacitive removal tested electrode was obtained via complete grinding the prepared material (40 mg), conductive carbon black, and polytetrafluoroethylene (PTFE) according to 8:1:1 mass ratio and painted on a square graphite film. The asymmetric system was made by using commercial activated carbon (AC) as the counter electrode and $W_{18}O_{49}$/Graphene and $W_{18}O_{49}$/C samples as the working electrode ($W_{18}O_{49}$/Graphene||AC, $W_{18}O_{49}$/C||AC). Another removal system (AC||AC) was obtained by using activated carbon (40 mg) as the working and counter electrodes (40 mg). The nonconductive spacer layer was used to separate the positive and negative electrodes. 65 mL single metal ion solution or multi-metal ion mixed solution passed through the deionization device at 40 mL/min flow rate, and each desalination experiment was controlled at 1.2 V

for 120 min. The repetitive experiments of removal were tested for 5 times with the error of ± 1%. More experiments are showed in Supporting Information.

Results and Discussion

Structure and Composition Analysis. The detailed synthesis route of the $W_{18}O_{49}$/Graphene material is shown in Figure S1. The morphology and structure of the obtained material were analyzed by SEM and TEM. The SEM images show that $W_{18}O_{49}$/C has a layered spherical structure (Figure S2), while $W_{18}O_{49}$/Graphene presents a layered ball-flower-like structure (Figure S3). This is because the graphene is coated on the outside of $W_{18}O_{49}$, thus forming graphene lamellar ball flowers. The TEM images (Figure S3-4) also reveal that the ball-flower shaped structure is composed of the graphene lamellar structure. The HRTEM image (Figure S4) further show that the ball-flower structure has the wrinkled characteristics of graphene. Meanwhile, the lattice stripes (3.7Å) of $W_{18}O_{49}$ are displayed in the inner layer. The selected area electron diffraction (SAED) diagram (Figure S4d) also confirms many small polycrystalline $W_{18}O_{49}$ particles in the inner layer region. The element types of the materials were further observed via energy dispersive X-ray spectroscopy (EDS). The results of EDS mapping (Figure S3) and line scans (Figure S5) reveal that W, O and C were distributed in the materials. It suggests that graphene forms a conductive channel between $W_{18}O_{49}$ nanoparticles, which is expected to improve the electrochemical performance.

The pore structure of the materials was calculated by the nitrogen isotherm analysis. The specific surface areas of $W_{18}O_{49}$/C and $W_{18}O_{49}$/Graphene are 181 m^2/g and 218 m^2/g (Table S1). This is because the graphene lamellar structure of $W_{18}O_{49}$ nanoparticles increases the specific surface area. The BET curve of the materials has a hysteresis line in the high-pressure region (Figure S6), indicating the existence of mesopore in the material. At the same time, the adsorption capacity of N_2 increases rapidly

at low pressure, which confirms the existence of micropores. From the pore size distribution curves, $W_{18}O_{49}$/Graphene has a larger total pore volume (Table S1). In addition, contact angle analysis proved that $W_{18}O_{49}$/Graphene is more hydrophilic than $W_{18}O_{49}$/C and AC (Figure S7).

The composition of the materials was determined by X-ray diffractometer (XRD) measurement. The XRD patterns showed that all samples have sharp peaks of $W_{18}O_{49}$. The sharp peak strongly indicates that the sample is essentially crystalline, which can be indexed by the hexagonal crystal structure of $W_{18}O_{49}$ with space group P2/m. A small amount of graphene exists in $W_{18}O_{49}$/Graphene, but no peak corresponding to the original graphene is observed in $W_{18}O_{49}$/Graphene samples. The Raman spectra confirm the amorphous properties of the $W_{18}O_{49}$ (Figure S8). The four main peaks at 128 cm^{-1}, 253 cm^{-1}, 695 cm^{-1} and 802 cm^{-1} are the typical characteristics of the monoclinic phase structure of $W_{18}O_{49}$, which are consistent with the XRD results. Meanwhile, the peaks of 1362 cm^{-1} (D band) correspond to the sp^3 hybrid carbon and the peaks of 1584 cm^{-1} (G band) correspond to the sp^2 hybrid carbon. The integral area ratio (I_D/I_G) of D band and G band is related to the degree of disorder of the sample. The higher the I_D/I_G ratio represented the higher the degree of disorder of the material. The higher I_D/I_G ratio is beneficial to electronic conductivity and electrolyte transport. The results show that the $W_{18}O_{49}$/Graphene material has a higher I_D/I_G ratio than $W_{18}O_{49}$/C and AC (Table S2).

The surface chemical states of $W_{18}O_{49}$/Graphene were tested by X-ray photoelectron spectroscopy (XPS). The general XPS spectrum of $W_{18}O_{49}$/Graphene shows the peaks of $C_{1s,}$ O_{1s}, and W_{4f} (Figure S9, Table S3). Simultaneously, the high-resolution O_{1s} spectra demonstrates the existence of W-O bond (Figure S10). Besides, the high-resolution W_{4f} spectra at 35.4 and 37.6 eV can be attributed to the W^{5+}. The W_{4f} spectra at 34.5 and 36.7 eV belong to the W^{4+}. The $W4f_{7/2}$ at 38.1 eV and $W4f_{5/2}$ at 35.9 eV are consistent with the values of W^{6+}.

Electrochemical Performance. Cyclic voltammetry (CV) measurements of $W_{18}O_{49}$/Graphene, $W_{18}O_{49}$/C, and AC were conducted at different sweeping speeds in the 1000 mg/L NaCl solution (Figure S11, S15-17). The result shows that $W_{18}O_{49}$/Graphene has a rectangular closing curve and good capacitor characteristics by electro-adsorption. The specific capacitance of $W_{18}O_{49}$/Graphene is 120 F/g at the scanning rate of 1 mV/s, which is superior to those of other electrodes, indicating that it has a larger adsorption capacity. The specific capacitance was further tested by charging and discharging at various current densities in the 1000 mg/L NaCl solution. It shows that $W_{18}O_{49}$/Graphene has the highest specific capacitance 564 F/g at the current density of 0.2 A/g (Figure S12, S15-17). Furthermore, the $W_{18}O_{49}$/Graphene electrode has excellent stability after 10000 cycles (Figure S13). The electrochemical impedance spectroscopy (EIS) test shows a smaller charge transfer resistance of $W_{18}O_{49}$/Graphene (Figure S14). This may be due to the high electrical conductivity of $W_{18}O_{49}$/Graphene by graphene coating. The slope of the EIS curve is positively correlated to the capacitance characteristics. The results show that $W_{18}O_{49}$/Graphene curve has the largest slope, indicating that the capacitor has the best performance.

Capacitive Removal of Heavy Metal Ions from Wastewater. We explored the ability of $W_{18}O_{49}$/Graphene||AC electrodes to remove a variety of heavy metal ions from wastewater in the single, binary, and multi-component systems via the electro-adsorption and electro-reaction coupling process in asymmetric deionization system (Figure 1). The $W_{18}O_{49}$/Graphene electrodes can reach close to 99% removal efficiency of heavy metal ions in the low-concentration single-component metal nitrate solution (10 mg/L). Meanwhile, the electrode exhibits a high removal efficiency of Cr^{3+} (96%), Cd^{2+} (92%), Pb^{2+} (92%), Ni^{2+} (93%), Co^{2+} (94%), Cu^{2+} (98%), and Fe^{3+} (95%) in the high-concentration single-component metal nitrate solution (50 mg/L) (Figure 2a). To explore the practical application of

electrode, the $W_{18}O_{49}$/Graphene electrodes were used to test the removal efficiency of heavy metal ions in the complex solutions. The removal efficiency of heavy metal ions with $W_{18}O_{49}$/Graphene electrode was explored at 1.2 V in complex binary-component solutions containing a metal nitrate and NaCl. The removal efficiency of Na^+ ion is less than 30% (Figure 2b), but the removal efficiency of heavy metal ions could keep at 99% in low-concentration heavy metal ions solutions (metal nitrate (10 mg/L) and NaCl (100 mg/L)) (Table S5). This may be due to the special lattice structure of $W_{18}O_{49}$, which makes the removal of sodium ions via the electro-adsorption and the removal of heavy metal ions via the electro-adsorption and electro-reaction coupling process. Meanwhile, the removal efficiency of heavy metal ions can be close to 90% in the high concentration (metal nitrate (50 mg/L) and NaCl (100 mg/L)) mixtures (Table S6). Furthermore, the removal efficiency of various heavy metal ions with $W_{18}O_{49}$/Graphene also be tested in a multi-component solution containing all the seven metal nitrates and NaCl. The removal efficiency of Na^+ ion is close to 20%, but the removal efficiency of heavy metal ions can reach 99% in the 10 mg/L for each metal nitrates and 100 mg/L NaCl multi-component solution (Figure 3a, Figure S28, Table S7) or 10 mg/L for each metal nitrates and 500 mg/L NaCl multi-component solution (Figure 3b, Table S8). Even the removal efficiency of heavy metal ions can be maintained at more than 90% in mixtures with the 50 mg/L for each metal nitrates and 100 mg/L NaCl multi-component solution (Table S9) or 50 mg/L for each metal nitrates and 500 mg/L NaCl multi-component solution (Table S10). In order to investigate the recyclability of the $W_{18}O_{49}$/Graphene electrode, a 120-min adsorption experiment was carried out in the multi-component solution containing all the seven metal nitrates (10 mg/L for each) and 100 mg/L NaCl at a constant voltage of 1.2 V and was followed by a 120-min short-circuit desorption experiment at the voltage of 0 V (short-circuit desorption experiment: a wire connects cathode and anode at the same time). The

adsorbed electrode was then soaked in ultrapure water and the solution is slippery until the electrical conductivity of the solution reaches the electrical conductivity of water. In each cycle test, the adsorbed solution was detected by inductively coupled plasma-optical emission spectrometer (ICP-OES) after 120 min. The result of regeneration experiment showed the electrode can maintain a good removal efficiency of heavy metal ions after 20 cycles (Figure 3c, Table S11). Additionally, the relative stability of pH in the solution indicates that there is no Faraday side reaction in the solutions. (Figure S29). The excellent recyclability indicates that the $W_{18}O_{49}$/Graphene electrode has great potential in practical applications of wastewater treatment. Moreover, the effect of pH values of the solution on the performance of the electrode is also explored. The electrode was immersed in different solutions with the pH value of 4-8 for 120 min, and then tested by XRD. The results showed that the electrode material still retains the original crystal diffraction structure of $W_{18}O_{49}$ (Figure S30). This indicates that $W_{18}O_{49}$ does not react with acids or alkaline. Meanwhile, we tested the solution pH values during the adsorption process in the multi-component solution containing all the seven metal nitrates (10 mg/L for each) and 100 mg/L NaCl at a constant voltage of 1.2 V. When the pH value of solution is closed to 6, the removal efficiency of heavy metal ions can reach 99%. However, when the pH value > 6, the removal efficiency of heavy metal ions decreases. This is because alkali reacts with heavy metal ions to form precipitation, thus reducing the removal efficiency (Figure S31).

Furthermore, we also explored the effect of organic compounds on the removal efficiency of heavy metal ions. The removal efficiency of various pollutants with the electrode was tested in the multi-component solution containing all the seven metal nitrates (10 mg/L for each), 100 mg/L NaCl and 20 mg/L aniline solutions or the multi-component solution containing all the seven metal nitrates (10 mg/L for each), 100 mg/L NaCl and 20 mg/L methyl blue solutions at a constant voltage of 1.2 V for

120 min. The concentration of heavy metal ions was tested by ICP-OES. The concentration of aniline and methyl blue was tested by UV–vis spectrophotometer. The results revealed that the removal efficiency of heavy metal ions still maintain 99% in the above two mixed solutions and the removal efficiency of aniline and methyl blue is closed to 100% (Figure S32-33). Therefore, the electrode has high removal efficiency for heavy metal ions in wastewater in the presence of organic pollutants.

Besides, the removal efficiency of $W_{18}O_{49}$/Graphene electrode for various heavy metal ions was tested at 1.2 V in heavy metal ions and $CaCl_2$ mixed solution. The results revealed that the removal efficiency of Ca^{2+} was less than 30%, but the SCR efficiency of heavy metal ions in the multi-component solution containing all the seven metal nitrates (10 mg/L for each) and 100 mg/L $CaCl_2$ could be close to 100% (Table S12). The SCR efficiency of heavy metal ions could keep 99% in the multi-component solution containing all the seven metal nitrates (10 mg/L for each) and 500 mg/L $CaCl_2$ (Table S13). We tested the CV curve of the electrode in 100 mg/L $CaCl_2$ solution. The electrode does not show pseudo-capacitance effect at the sweep rate of 0.2 mV/s, which indicates that the adsorption of Ca ions is also electro-adsorption (Figure S34). This showed that the $W_{18}O_{49}$/Graphene have outstanding SCR efficiency of heavy metal ions.

The adsorption/desorption mechanisms of $W_{18}O_{49}$/Graphene were studied by XRD. The electrode has the diffraction peak of $W_{18}O_{49}$ after adsorption of heavy metal ions in single-component metal nitrate solutions or after Na-adsorbed in 100 mg/L NaCl solutions (Figure 4a, Figure S35-36). The original crystal structure is still maintained after the desorption of metal ions. Furthermore, the crystal structure characteristics of $W_{18}O_{49}$ could maintain by XRD detection after 5th, 10th, 15th and 20th ion removal and ion release cycle in the multi-component synthetic wastewater (Figure S37). This indicates that the heavy metal ions can be embedded and detached freely in the layered structure of the

electrode, which will not change the crystal structure of $W_{18}O_{49}$. The adsorbed and desorbed electrodes were also analyzed by Raman (Figure 4b). The results reveal that the vibration peak of the $W_{18}O_{49}$ crystal structure disappears after adsorption, and then appears again after desorption. This indicates the free movement of heavy metal ions within the layered framework of $W_{18}O_{49}$/Graphene. Meanwhile, the CV showed a pseudo-capacitance effect appears in the voltage range of −0.6 to 0.6 V in seven metal nitrates (100 mg/L for each) (Figure S38) and the multi-component solution containing all the seven metal nitrates (10 mg/L for each) and 100 mg/L NaCl (Figure 5a). However, there is no pseudo-capacitance effect in 100 mg/L NaCl solution. Therefore, the removal of sodium ions is mainly attributed to the electrostatic force of the EDL mechanism in the process of electro-adsorption. However, the removal of heavy metal ions is mainly through the coupling process of electro-adsorption and electro-reaction. In the removal process of heavy metal ions, the electro-adsorption contributed 47.43%, and the electro-reaction contributed 52.57% (Figure S39). Furthermore, the XPS spectra of $W_{18}O_{49}$/Graphene after adsorbing heavy metals ions in the multi-component synthetic wastewater confirm the increase of W^{5+} content and the decrease of W^{4+} content in the material (Figure 5c, Table S14). Nevertheless, the content of W in various valence states did not change after Na-adsorbed in 100 mg/L NaCl (Figure 5c). This indicates that the capacitive removal of heavy metal ions via the electro-adsorption and electro-reaction coupling process (Figure 5d). In addition, the in-situ Raman test was used to observe the insertion and extraction reaction of heavy metal ions in the multi-component synthetic wastewater via the CV test at 0.2 mV/s. The Raman spectra reveal that the electrode has the characteristic peaks of $W_{18}O_{49}$ crystal structure in the low voltage range (Figure 5a-b, 5d). The characteristic peaks of 128 cm^{-1}, 695 cm^{-1} and 802 cm^{-1} are attributed to the stretching vibration of the W-O bond, and the other peaks at 253 cm^{-1} belong to the bending vibration of the O-W-O bond which

is related to the monoclinic phase. However, these characteristic peaks gradually disappear with the increase of voltage. This suggests that heavy metal ions are constantly inserted into the interlayer spacing of the electrode material, disrupting its original structural symmetry, and making these vibration modes disappear. Furthermore, these unique vibration characteristic peaks appear again with the decrease of the voltage, which indicates that the heavy metal ions are constantly detached from the electrode. As a result, the highly efficient removal of heavy metal ions via the electro-adsorption and electro-reaction coupling process can be well regulated by electrochemistry.

In summary, highly efficient removal of metal ions from wastewater over the electro-adsorption and electro-reaction coupling process was originally demonstrated. The $W_{18}O_{49}$/Graphene electrode demonstrated high removal efficiency of heavy metal ions in synthetic wastewater. These results suggest that the electrochemical systems equipped with the electro-adsorption and electro-reaction coupling process could be a feasible solution for desalting wastewater.

ASSOCIATED CONTENT

Supporting information

Information about the synthesis route, SEM images, TEM images and EDS of the $W_{18}O_{49}$/C and $W_{18}O_{49}$/Graphene materials (Figure S1-5); N_2 adsorption−desorption isotherms (Figure S6); Dynamic water contact angle (Figure S7); XRD of the $W_{18}O_{49}$/Graphene (Figure S30, S35-37); Raman of the $W_{18}O_{49}$/Graphene, $W_{18}O_{49}$/C, and AC materials (Figure S8); The XPS peaks of the materials (Figure S9-10); Electrochemical performance of the $W_{18}O_{49}$/Graphene, $W_{18}O_{49}$/C, and AC materials (Figure S11-17, S34, S38-39); Desalination Performance (Figure S18-27); The removal efficiency of heavy metal ions (Figure S28, S31); Plot of pH (Figure S29); The organic pollutant removal performance (Figure S32-33); Porous properties of the materials (Table S1); Summary of relative intensity ratios of

all materials in Raman spectra (Table S2); Elemental contents (Table S3); Removal rate with the state-of-the-art electrode materials (Table S4); Heavy metal ions concentration after sorption 120 min in mixed heavy metal ions solutions by ICP-OES tested (Table S5-13); The area corresponding to the peak position of XPS (Table S14).

Author Information

Corresponding Author

*E-mail: dszhang@shu.edu.cn; Tel: +86-21-66137152.

ORCID ID

Dengsong Zhang: 0000-0003-4280-0068

Notes

There are no conflicts to declare.

ACKNOWLEDGMENTS

The authors acknowledge the support of the National Natural Science Foundation of China (21906101).

References

1. Elimelech, M.; Phillip, W. A., The future of seawater desalination: Energy, technology, and the environment. *Science* **2011**, *333*, 712-717.

2. Pekel, J.-F.; Cottam, A.; Gorelick, N.; Belward, A. S., High-resolution mapping of global surface water and its long-term changes. *Nature* **2016**, *540*, 418-422.

3. Yang, S.; Hu, J.; Chen, C.; Shao, D.; Wang, X., Mutual effects of Pb(II) and humic acid adsorption on multiwalled carbon nanotubes/polyacrylamide composites from aqueous solutions. *Environ. Sci. Technol.* **2011**, 45, 3621-3627.

4. Zhang, Y.; Zhang, S.; Chung, T. S., Nanometric graphene oxide framework membranes with enhanced heavy metal removal via nanofiltration. *Environ. Sci. Technol.* **2015**, 49, 10235-10242.

5. Dai, C.; Hu, Y., Fe(III) hydroxide nucleation and growth on quartz in the presence of Cu(II), Pb(II), and Cr(III): Metal hydrolysis and adsorption. *Environ. Sci. Technol.* **2015**, 49, 292-300.

6. Chen, Z.; Liang, Y.; Jia, D. S.; Chen, W. Y.; Cui, Z. M.; Wang, X. K., Layered silicate RUB-15 for efficient removal of UO_{22}^{+} and heavy metal ions by ion-exchange. *Environ. Sci-Nano.* **2017**, 4, 1851-1858.

7. Zhang, C. Y.; Wu, L.; Ma, J. X.; Pham, A. N.; Wang, M.; Waite, T. D., Integrated flow-electrode capacitive deionization and microfiltration system for continuous and energy-efficient brackish water desalination. *Environ. Sci. Technol.* **2019**, *53*, 13364-13373.

8. Zhang, X.; Zuo, K.; Zhang, X.; Zhang, C.; Liang, P., Selective ion separation by capacitive deionization (CDI) based technologies: a state-of-the-art review. *Environ. Sci. Water. Res. Technol.* **2020**, *6*, 243-257.

9. Srimuk, P.; Su, X.; Yoon, J.; Aurbach, D.; Presser, V., Charge-transfer materials for electrochemical water desalination, ion separation and the recovery of elements. *Nat. Rev. Mater.* **2020**, *5*, 517-538.

10. Han, J.; Yan, T.; Shen, J.; Shi, L.; Zhang, J.; Zhang, D., Capacitive deionization of saline water by using MoS_2-graphene hybrid electrodes with high volumetric adsorption capacity. *Environ. Sci. Technol.* **2019**, *53*, 12668-12676.

11. Li, B.; Zheng, T.; Ran, S.; Sun, M.; Shang, J.; Hu, H.; Lee, P.-H.; Boles, S. T., Performance recovery in degraded carbon-based electrodes for capacitive deionization. *Environ. Sci. Technol.* **2020**, *54*, 1848-1856.

12. Guyes, E. N.; Malka, T.; Suss, M. E., Enhancing the ion-size-based selectivity of capacitive deionization electrodes. *Environ. Sci. Technol.* **2019**, *53*, 8447-8454.

13. Hatzell, K. B.; Boota, M.; Gogotsi, Y., Materials for suspension (semi-solid) electrodes for energy and water technologies. *Chem. Soc. Rev.* **2015**, *44*, 8664-8687.

14. Hawks, S. A.; Ramachandran, A.; Porada, S.; Campbell, P. G.; Suss, M. E.; Biesheuvel, P. M.; Santiago, J. G.; Stadermann, M., Performance metrics for the objective assessment of capacitive deionization systems. *Water. Res.* **2019**, *152*, 126-137.

15. Tang, W.; Liang, J.; He, D.; Gong, J.; Tang, L.; Liu, Z.; Wang, D.; Zeng, G., Various cell architectures of capacitive deionization: Recent advances and future trends. *Water. Res.* **2019**, *150*, 225-251.

16. Su, X.; Tan, K.-J.; Elbert, J.; Ruettiger, C.; Gallei, M.; Jamison, T. F.; Hatton, T. A., Asymmetric Faradaic systems for selective electrochemical separations. *Energy. Environ. Sci.* **2017**, *10*, 1272-1283.

17. Khan, Z. U.; Yan, T.; Han, J.; Shi, L.; Zhang, D., Capacitive deionization of saline water using graphene nanosphere decorated N-doped layered mesoporous carbon frameworks. *Environ. Sci-Nano.* **2019**, *6*, 3442-3453.

18. Chen, R.; Sheehan, T.; Ng, J. L.; Brucks, M.; Su, X., Capacitive deionization and electrosorption for heavy metal removal. *Environ. Sci-Wat. Res.* **2020**, *6*, 258-282.

19. Wang, G.; Yan, T.; Zhang, J.; Shi, L.; Zhang, D., Trace-Fe-enhanced capacitive deionization of saline water by boosting electron transfer of electro-adsorption sites. *Environ. Sci. Technol.* **2020**, *54*, 8411-8419.

20. Wang, H.; Yan, T.; Shen, J.; Zhang, J.; Shi, L.; Zhang, D., Efficient removal of metal ions by capacitive deionization with straw waste derived graphitic porous carbon nanosheets. *Environ. Sci-*

354 *Nano.* **2020**, *7*, 317-326.

355 21. Zhang, J.; Yan, T.; Fang, J.; Shen, J.; Shi, L.; Zhang, D., Enhanced capacitive deionization of saline
356 water using N-doped rod-like porous carbon derived from dual-ligand metal-organic frameworks.
357 *Environ. Sci-Nano.* **2020**, *7*, 926-937.

358 22. Zeng, X.; Wang, G.; Liu, Y.; Zhang, X., Graphene-based antimicrobial nanomaterials: Rational
359 design and applications for water disinfection and microbial control. *Environ. Sci-Nano.* **2017**, *4*, 2248-
360 2266.

361 23. Hemmatifar, A.; Ramachandran, A.; Liu, K.; Oyarzun, D. I.; Bazant, M. Z.; Santiago, J. G.,
362 Thermodynamics of ion separation by electrosorption. *Environ. Sci. Technol.* **2018**, *52*, 10196-10204.

363 24. Yan, T.; Liu, J.; Lei, H.; Shi, L.; An, Z.; Park, H. S.; Zhang, D., Capacitive deionization of saline
364 water using sandwich-like nitrogen-doped graphene composites via a self-assembling strategy.
365 *Environ. Sci-Nano.* **2018**, *5*, 2722-2730.

366 25. Hsu, C.-C.; Tu, Y.-H.; Yang, Y.-H.; Wang, J.-A.; Hu, C.-C., Improved performance and long-term
367 stability of activated carbon doped with nitrogen for capacitive deionization. *Desalination.* **2020**, *481*,
368 114362.

369 26. Liu, P. Y.; Yan, T. T.; Zhang, J. P.; Shi, L. Y.; Zhang, D. S., Separation and recovery of heavy metal
370 ions and salt ions from wastewater by 3D graphene-based asymmetric electrodes via capacitive
371 deionization. *J. Mater. Chem. A.* **2017**, *5*, 14748-14757.

372 27. Tang, W.; Wang, X.; Zeng, G.; Liang, J.; Li, X.; Xing, W.; He, D.; Tang, L.; Liu, Z., Electro-
373 assisted adsorption of Zn(II) on activated carbon cloth in batch-flow mode: Experimental and
374 theoretical investigations. *Environ. Sci. Technol.* **2019**, *53*, 2670-2678.

375 28. Ganganboina, A. B.; Doong, R.-A., Nitrogen doped graphene quantum dot-decorated earth-

376 abundant nanotubes for enhanced capacitive deionization. *Environ. Sci-Nano.* **2020**, *7*, 228-237.
377 29. Zhang, Q.; Huang, Y.; Xia, D.; Hu, L.; Li, P.; Tan, L.; Wang, Y.; He, C.; Shu, D.; Xie, X., High-
378 performance water desalination of heteroatom nitrogen- and sulfur-codoped open hollow tubular
379 porous carbon electrodes via capacitive deionization. *Environ. Sci-Nano.* **2019**, *6*, 3359-3373.
380 30. Hawks, S. A.; Ceron, M. R.; Oyarzun, D. I.; Pham, T. A.; Zhan, C.; Loeb, C. K.; Mew, D.; Deinhart,
381 A.; Wood, B. C.; Santiago, J. G.; Stadermann, M.; Campbell, P. G., Using ultramicroporous carbon for
382 the selective removal of nitrate with capacitive deionization. *Environ. Sci. Technol.* **2019**, *53*, 10863-
383 10870.
384 31. Lu, S.; Hu, Y.; Wan, S.; McCaffrey, R.; Jin, Y.; Gu, H.; Zhang, W., Synthesis of ultrafine and highly
385 dispersed metal nanoparticles confined in a thioether-containing covalent organic framework and their
386 catalytic applications. *J. Am. Chem. Soc.* **2017**, *139*, 17082-17088.
387 32. Kang, J. S.; Kim, S.; Chung, D. Y.; Son, Y. J.; Jo, K.; Su, X.; Lee, M. J.; Joo, H.; Hatton, T. A.;
388 Yoon, J.; Sung, Y. E., Rapid inversion of surface charges in heteroatom-doped porous carbon: A route
389 to robust electrochemical desalination. *Adv. Funct. Mater.* **2020**, *30*, 1909387.
390 33. Hu, S.; Xie, K.; Zhang, X.; Zhang, S.; Gao, J.; Song, H.; Chen, D., Significantly enhanced
391 capacitance deionization performance by coupling activated carbon with triethyltetramine-
392 functionalized graphene. *Chem. Eng. J.* **2020**, *384*, 123317.
393 34. Liu, T.; Serrano, J.; Elliott, J.; Yang, X.; Cathcart, W.; Wang, Z.; He, Z.; Liu, G., Exceptional
394 capacitive deionization rate and capacity by block copolymer-based porous carbon fibers. *Sci. Adv.*
395 **2020**, *6*, eaaz0906.
396 35. Wang, L.; Dykstra, J. E.; Lin, S., Energy efficiency of capacitive deionization. *Environ. Sci.*
397 *Technol.* **2019**, *53*, 3366-3378.

36. Wang, H.; Mi, X. Y.; Li, Y.; Zhan, S. H., 3D graphene-based macrostructures for water treatment. *Adv. Mater.* **2020**, *32*, 1806843.

37. Liu, P.; Yan, T.; Shi, L.; Park, H. S.; Chen, X.; Zhao, Z.; Zhang, D., Graphene-based materials for capacitive deionization. *J. Mater. Chem. A.* **2017**, *5*, 13907-13943.

38. Zhao, Y.; Liu, J.; Hu, Y.; Cheng, H.; Hu, C.; Jiang, C.; Jiang, L.; Cao, A.; Qu, L., Highly compression-tolerant supercapacitor based on polypyrrole-mediated graphene foam electrodes. *Adv. Mater.* **2013**, *25*, 591-595.

39. Xu, Y.; Sheng, K.; Li, C.; Shi, G., Self-assembled graphene hydrogel via a one-step hydrothermal process. *ACS Nano.* **2010**, *4*, 4324-4330.

40. Xu, Y.; Lin, Z.; Huang, X.; Wang, Y.; Huang, Y.; Duan, X., Functionalized graphene hydrogel-based high-performance supercapacitors. *Adv. Mater.* **2013**, *25*, 5779.

41. Kim, K.; Cotty, S.; Elbert, J.; Chen, R. L.; Hou, C. H.; Su, X., Asymmetric redox-polymer interfaces for electrochemical reactive separations: Synergistic capture and conversion of arsenic. Adv. Mater. **2020**, 32, 1906877.

42. Mao, M.; Yan, T.; Chen, G.; Zhang, J.; Shi, L.; Zhang, D., Selective capacitive removal of Pb^{2+} from wastewater over redox-active electrodes. *Environ. Sci. Technol.* **2021**, *55*, 730-737.

43. Shen, X.; Xiong, Y.; Hai, R.; Yu, F.; Ma, J., All-MXene-based integrated membrane electrode constructed using $Ti_3C_2T_x$ as an intercalating agent for high-performance desalination. *Environ. Sci. Technol.* **2020**, 5*4*, 4554-4563.

44. Ma, J.; Xiong, Y.; Dai, X.; Yu, F., Zinc spinel ferrite nanoparticles as a pseudocapacitive electrode with ultrahigh desalination capacity and long-term stability. *Environ. Sci. Tech. Let.* **2020**, *7*, 118-125.

45. Zhang, C.; He, D.; Ma, J.; Tang, W.; Waite, T. D., Faradaic reactions in capacitive deionization

(CDI)- problems and possibilities: A review. *Water. Res.* **2018**, *128*, 314-330.

46. Yu, F.; Wang, L.; Wang, Y.; Shen, X.; Cheng, Y.; Ma, J., Faradaic reactions in capacitive deionization for desalination and ion separation. *J. Mater. Chem. A.* **2019**, *7*, 15999-16027.

47. Hand, S.; Cusick, R. D., Characterizing the impacts of deposition techniques on the performance of MnO_2 cathodes for sodium electrosorption in hybrid capacitive deionization. *Environ. Sci. Technol.* **2017**, *51*, 12027-12034.

48. Son, M.; Pothanamkandathil, V.; Yang, W.; Vrouwenvelder, J. S.; Gorski, C. A.; Logan, B. E., Improving the thermodynamic energy efficiency of battery electrode deionization using flow-through electrodes. *Environ. Sci. Technol.* **2020**, *54*, 3628-3635.

49. Liu, T.; Yuan, J.; Zhang, B.; Liu, W.; Lin, L.; Meng, Y.; Yin, S.; Liu, C.; Luan, F., Removal and recovery of uranium from groundwater using direct electrochemical reduction method: Performance and implications. *Environ. Sci. Technol.* **2019**, 53, 14612-14619.

50. Cao, J.; Wang, Y.; Wang, L.; Yu, F.; Ma, J., $Na_3V_2(PO_4)_3$@C as faradaic electrodes in capacitive deionization for high-performance desalination. *Nano. Lett.* **2019**, *19*, 823-828.

51. Lee, J.; Kim, S.; Kim, C.; Yoon, J., Hybrid capacitive deionization to enhance the desalination performance of capacitive techniques. *Energy. Environ. Sci.* **2014**, *7*, 3683-3689.

52. Ding, L.; Li, L.; Liu, Y.; Wu, Y.; Lu, Z.; Deng, J.; Wei, Y.; Caro, J.; Wang, H., Effective ion sieving with $Ti_3C_2T_x$ MXene membranes for production of drinking water from seawater. *Nat. Sustain.* **2020**, *3*, 296-302.

53. Liu, B. J.-W.; Zheng, J.; Wang, J.-L.; Xu, J.; Li, H.-H.; Yu, S.-H., Ultrathin $W_{18}O_{49}$ nanowire assemblies for electrochromic devices. *Nano Lett.* **2013**, *13*, 3589-3593.

54. Huang, Z.-F.; Song, J.; Wang, X.; Pan, L.; Li, K.; Zhang, X.; Wang, L.; Zou, J.-J., Switching charge

442 transfer of $C_3N_4/W_{18}O_{49}$ from type-II to Z-scheme by interfacial band bending for highly efficient
443 photocatalytic hydrogen evolution. *Nano Energy.* **2017**, *40*, 308-316.
444 55. Zhang, N.; Jalil, A.; Wu, D.; Chen, S.; Liu, Y.; Gao, C.; Ye, W.; Qi, Z.; Ju, H.; Wang, C.; Wu, X.;
445 Song, L.; Zhu, J.; Xiong, Y., Refining defect states in $W_{18}O_{49}$ by Mo doping: A strategy for tuning N_2
446 activation towards solar-driven nitrogen fixation. *J. Am. Chem. Soc.* **2018**, *140*, 9434-9443.
447

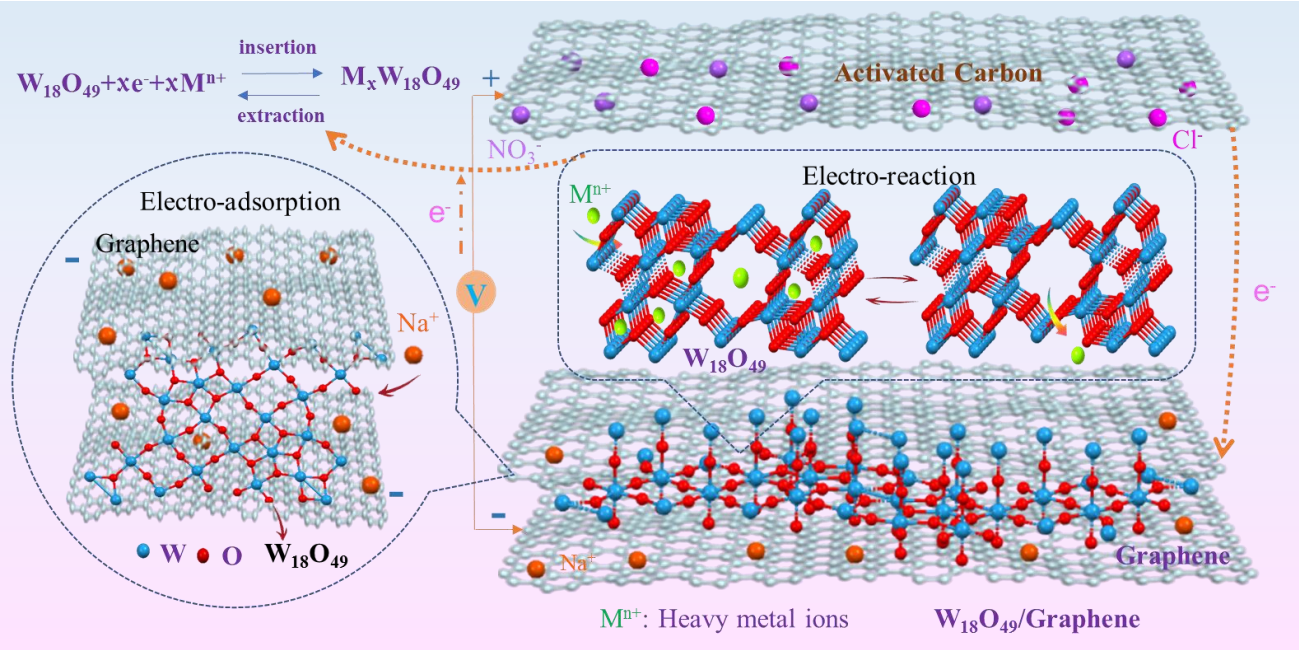

Figure 1. Schematic illustration of the electro-adsorption and electro-reaction coupling process.

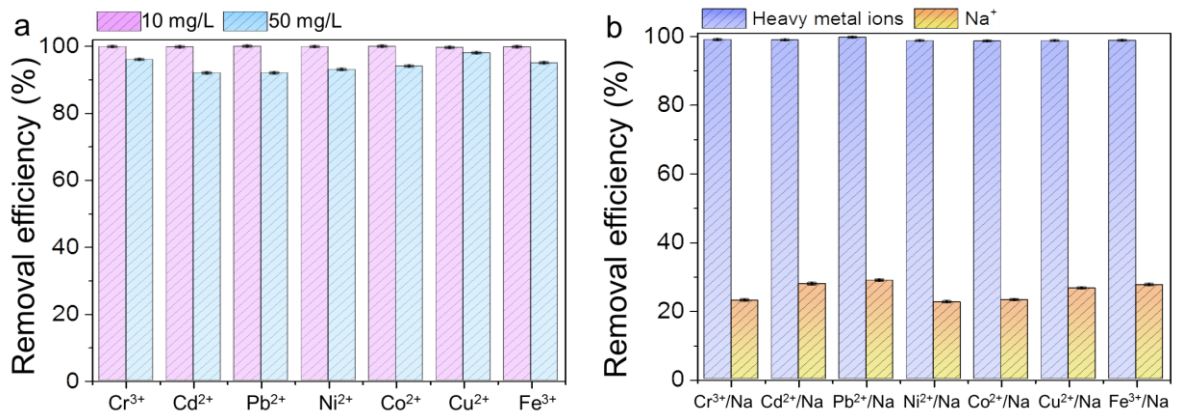

451

452 **Figure 2.** (a) Plots of removal efficiency of heavy metal ions after 120 min of capacitive adsorption in

453 the single-component metal nitrate solution (10 mg/L for each or 50 mg/L for each) at 1.2 V. (b) Plots

454 of removal efficiency of heavy metal ions and Na^+ with the $W_{18}O_{49}$/Graphene||AC electrode after 120

455 min of capacitive adsorption in the binary-component solutions containing a metal nitrate (10 mg/L)

456 and NaCl (100 mg/L) at 1.2 V.

457

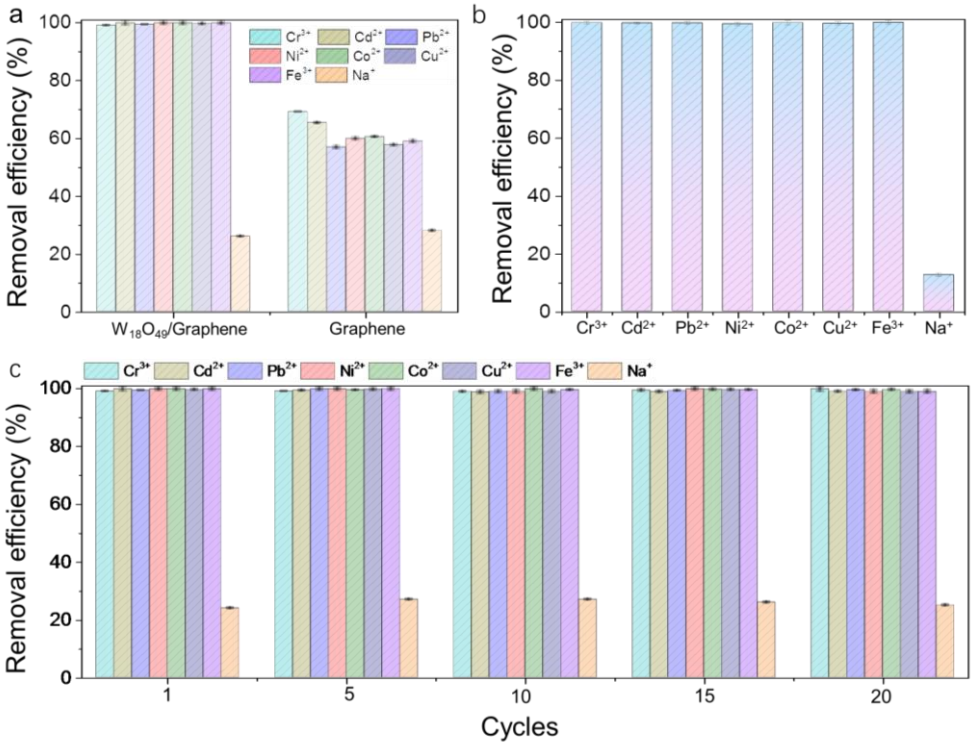

458

459 **Figure 3.** (a) Plots of removal efficiency of heavy metal ions and Na^+ with the $W_{18}O_{49}$/Graphene||AC
460 electrode and Graphene||AC electrode after 120 min of capacitive adsorption in the multi-component
461 solution containing all the seven metal nitrates (10 mg/L for each) and NaCl (100 mg/L) at 1.2 V. (b)
462 Plots of removal efficiency of heavy metal ions with the $W_{18}O_{49}$/Graphene||AC electrode after 120 min
463 of capacitive adsorption in the multi-component solution containing all the seven metal nitrates (10
464 mg/L for each) and NaCl (500 mg/L) at 1.2 V. (c) Recyclability of the $W_{18}O_{49}$/Graphene electrode in
465 the multi-component solution containing all the seven metal nitrates (10 mg/L for each) and NaCl (100
466 mg/L) at 1.2 V.

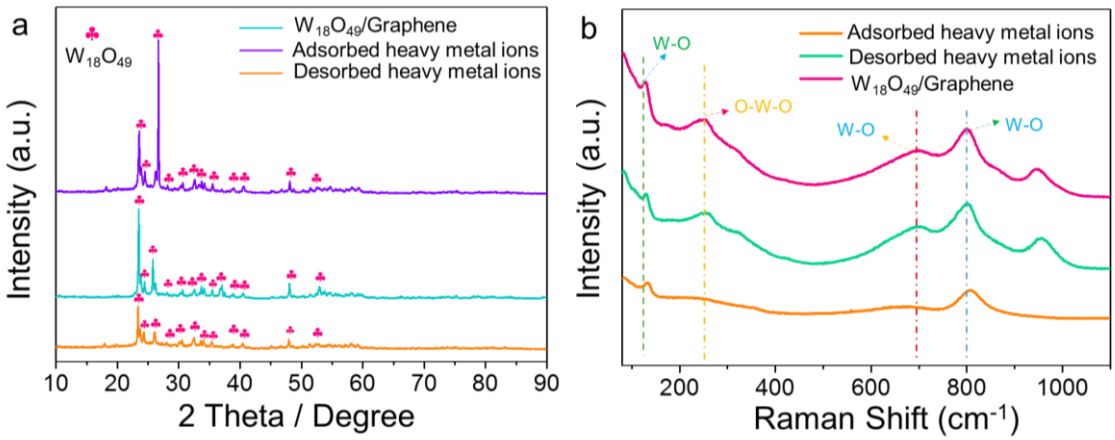

467

468 **Figure 4.** (a) XRD patterns of $W_{18}O_{49}$/Graphene before and after heavy metal ion adsorption in the

469 multi-component solution containing all the seven metal nitrates (10 mg/L for each) and 100 mg/L

470 NaCl at a constant voltage of 1.2 V. (b) Raman spectra of $W_{18}O_{49}$/Graphene electrode and after heavy

471 metal ions-adsorption and heavy metal ions-desorption in the multi-component solution containing all

472 the seven metal nitrates (10 mg/L for each) and 100 mg/L NaCl at a constant voltage of 1.2 V.

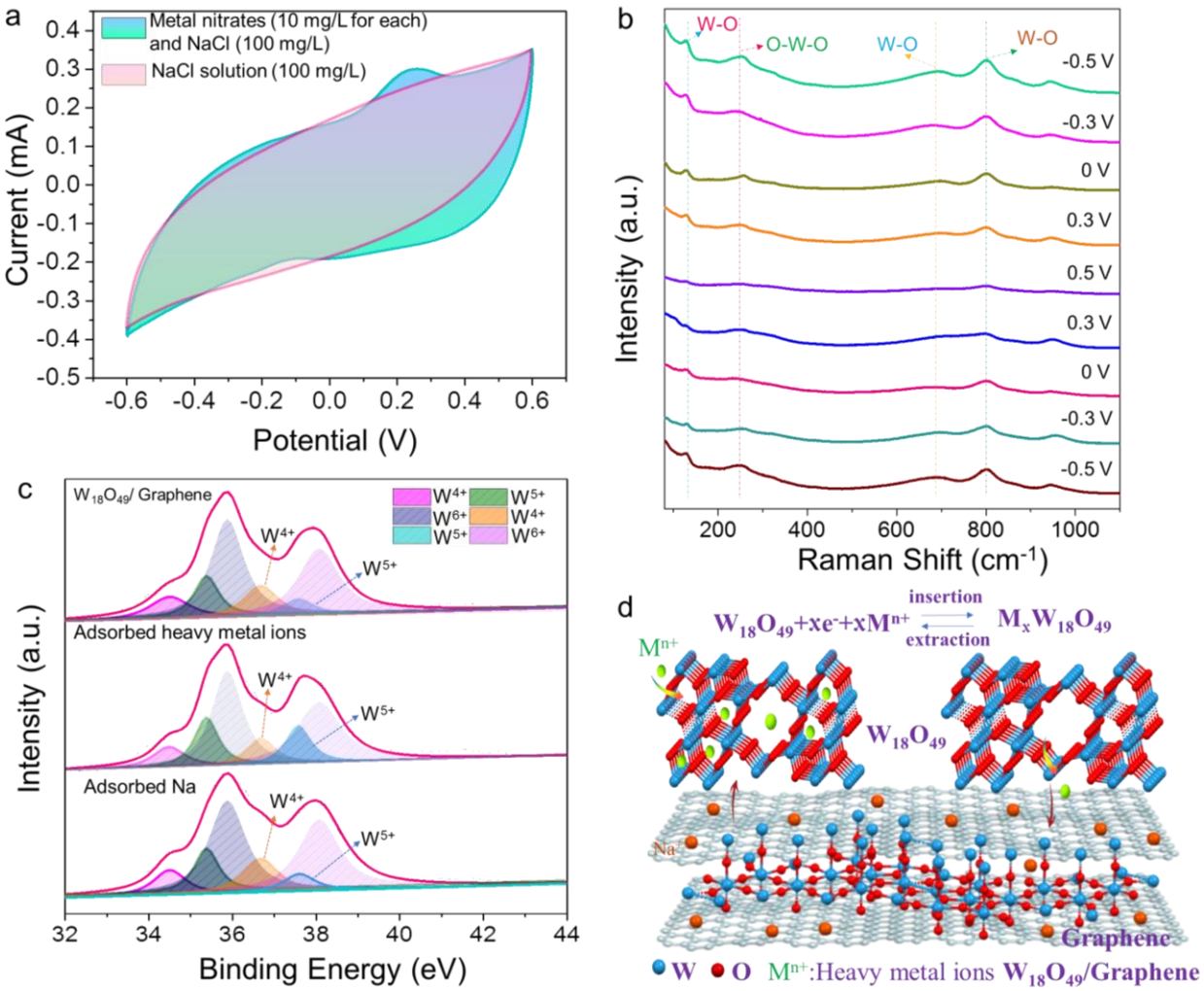

Figure 5. (a) CV curves of the $W_{18}O_{49}$/Graphene electrodes at 0.2 mV/s in the multi-component solution containing all the seven metal nitrates (10 mg/L for each) and 100 mg/L NaCl and at 0.2 mV/s in 100 mg/L NaCl at a constant voltage of 1.2 V. (b) In-situ Raman spectra of the $W_{18}O_{49}$/Graphene electrode at the CV scanning rate of 0.2 mV/s in the voltage range of −0.6~0.6. (c) W_{4f} spectra of the $W_{18}O_{49}$/Graphene electrodes, W_{4f} spectra of the $W_{18}O_{49}$/Graphene electrodes after Na-adsorbed in 100 mg/L NaCl at a constant voltage of 1.2 V and W_{4f} spectra of the $W_{18}O_{49}$/Graphene electrodes after heavy metal ions-adsorbed in the multi-component solution containing all the seven metal nitrates (10 mg/L for each) and 100 mg/L NaCl at a constant voltage of 1.2 V. (d) Schematic diagram of the electro-adsorption and electro-reaction coupling process on the surface of the $W_{18}O_{49}$/Graphene materials.

483

TOC

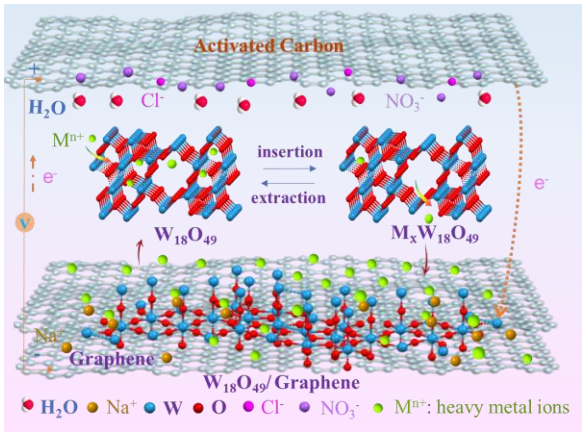
Activated Carbon
H_2O
Cl^-
NO_3^-
M^{n+}
e^-
insertion
extraction
$W_{18}O_{49}$
$M_xW_{18}O_{49}$
Na^+
Graphene
$W_{18}O_{49}$/ Graphene
H_2O Na^+ W O Cl^- NO_3^- M^{n+}: heavy metal ions

484